


CFP1 governs uterine epigenetic landscapes to intervene in progesterone responses for uterine physiology and suppression of endometriosis

Received: 14 November 2022

Accepted: 24 May 2023

Published online: 03 June 2023

 Check for updates

Seung Chel Yang^{1,10}, Mira Park^{1,10}, Kwon-Ho Hong², Hyeonwoo La², Chanhyeok Park², Peike Wang³, Gaizhen Li³, Qionghua Chen³, Youngsok Choi², Francesco J. DeMayo⁴, John P. Lydon⁵, David G. Skalnik⁶, Hyunjung J. Lim⁷, Seok-Ho Hong^{8,9}, So Hee Park¹, Yeon Sun Kim¹, Hye-Ryun Kim¹ & Haengseok Song¹✉

Progesterone (P₄) is required for the preparation of the endometrium for a successful pregnancy. P₄ resistance is a leading cause of the pathogenesis of endometrial disorders like endometriosis, often leading to infertility; however, the underlying epigenetic cause remains unclear. Here we demonstrate that CFP1, a regulator of H3K4me₃, is required for maintaining epigenetic landscapes of P₄-progesterone receptor (PGR) signaling networks in the mouse uterus. *Cfp1^{fl/fl};Pgr-Cre (Cfp1^{d/d})* mice showed impaired P₄ responses, leading to complete failure of embryo implantation. mRNA and chromatin immunoprecipitation sequencing analyses showed that CFP1 regulates uterine mRNA profiles not only in H3K4me₃-dependent but also in H3K4me₃-independent manners. CFP1 directly regulates important P₄ response genes, including *Gata2*, *Sox17*, and *Ihh*, which activate smoothed signaling pathway in the uterus. In a mouse model of endometriosis, *Cfp1^{d/d}* ectopic lesions showed P₄ resistance, which was rescued by a smoothed agonist. In human endometriosis, CFP1 was significantly downregulated, and expression levels between CFP1 and these P₄ targets are positively related regardless of PGR levels. In brief, our study provides that CFP1 intervenes in the P₄-epigenome-transcriptome networks for uterine receptivity for embryo implantation and the pathogenesis of endometriosis.

CXXC finger protein 1 (CFP1) is an important player in the epigenetic regulation of genes by inducing trimethylation at histone H3 lysine 4 (H3K4me₃) with SETD1, a histone methyltransferase¹. H3K4me₃ is mainly found in active promoters and turns chromatin into transcriptionally active euchromatin in the transcription start site (TSS) and CpG island (CGI)². When CFP1 binds to unmethylated CpG, it recruits SETD1A/B to trigger H3K4me₃ in the promoters of target

genes to increase gene expression^{1,3}. The deletion of CFP1, SETD1A, or SETD1B in mice caused embryonic lethality during or after gastrulation, suggesting the roles of SETD1-CFP1 complexes in early mammalian development^{4,5}. Furthermore, the conditional deletion of CFP1 highlighted that CFP1-associated H3K4me₃ has fundamental roles in various biological processes. CFP1-deficient embryonic stem cells failed to differentiate in vitro because of aberrant H3K4me₃ at

A full list of affiliations appears at the end of the paper. ✉ e-mail: hssong@cha.ac.kr

non-methylated CGI promoters, leading to transcriptional disturbance^{2,4,6}. CFPI plays an important role in intrathymic T-cell development and differentiation program of TH17 cells^{7,8}. Recent studies have also demonstrated that CFPI is required for epigenetic modification in non-replicative cells, such as germ cells, in mice^{9–11}.

The endometrium is a highly dynamic organ, and its function and cyclicity are mainly regulated by ovarian progesterone (P₄) and estrogen (E₂). Imbalances between P₄ and E₂ may cause various gynecological disorders such as endometriosis, repeated implantation failure, and endometrial cancer¹². P₄ and E₂ activate their nuclear receptors, progesterone receptors (PGRs), and estrogen receptors (ESRs) to control the expression of local factors for uterine functions. PGR-dependent signaling networks for epithelium–stroma interaction are necessary to promote uterine receptivity for embryo implantation and decidualization in the uterus¹³. The fine-tuning of epigenetic modulation is required for phase-specific transcriptional networks during the reproductive cycle, embryo implantation, and subsequent pregnancy^{14–16}. Dynamic changes in histone modifications occur during decidualization^{17,18}. Silencing and overexpression of EZH2, a histone methyltransferase for H3K27me₃, a repressive histone mark, disturb the expression of decidualization markers, such as IGFBP1 and PRL¹⁷. For successful parturition, biphasic modes of H3K27me₃ dynamics in decidual stromal cells dictate the regulated gene silencing in the uterine adaptation to pregnancy¹⁹. The acetylation and methylation patterns of H3 and H4 in women with endometriotic lesions are distinct from those of disease-free women²⁰. However, the physiological significance of epigenetic regulatory machineries, such as histone modification during early pregnancy and the pathogenesis of uterine disorders, remains largely unexplored.

Endometriosis is a disorder in which endometrial cells grow abnormally outside the uterus. The surgical removal of the ectopic endometrial lesion with hormonal suppression is the current standard of care; however, these therapies have a high incidence of relapse and various side effects^{21,22}. Endometriosis affects 10%–15% of women of reproductive age and is one of the leading causes of female infertility^{21–24}. Leading causes of endometriosis include increased E₂ response, P₄ resistance (decreased P₄ response), and/or abnormal epigenetic regulation^{25–28}. Although decreased P₄ response caused by reduced PGR expression is considered a main cause of endometriosis^{26,29}, the underlying cause of the decreased P₄ response, even with normal P₄ secretion and PGR expression, has not yet been elucidated.

Altered DNA methylation and histone modification on the genes for balanced hormone responses were mainly proposed to affect the endometrial function and the development of endometriosis^{9,12}. The loss of histone deacetylase 3 (HDAC3) is a result of failures in embryo implantation and decidualization and caused fibrosis in the endometrium, one of the symptoms of human endometriosis with reduced HDAC3 expression²⁵. However, epigenetic causes of how uterine cells grow outside the uterus in patients with endometriosis have not been clearly identified. Using a combination of genetic and pharmacologic tools and various analyses, we demonstrated that CFPI-dependent epigenetic regulation is necessary to maintain uterine transcriptional landscapes for P₄ response for a successful pregnancy and prevent endometriosis with P₄ resistance. Thus, this study provides fundamental insight into understanding the complex interplay between the P₄-PGR signaling pathway and uterine epigenome–transcriptome under physiologic and pathophysiologic conditions, such as endometriosis.

Results

Loss of *Cfp1* leads to infertility with multiple failures in oviductal embryo transport, P₄ uterine responses, embryo implantation, and decidualization in mice

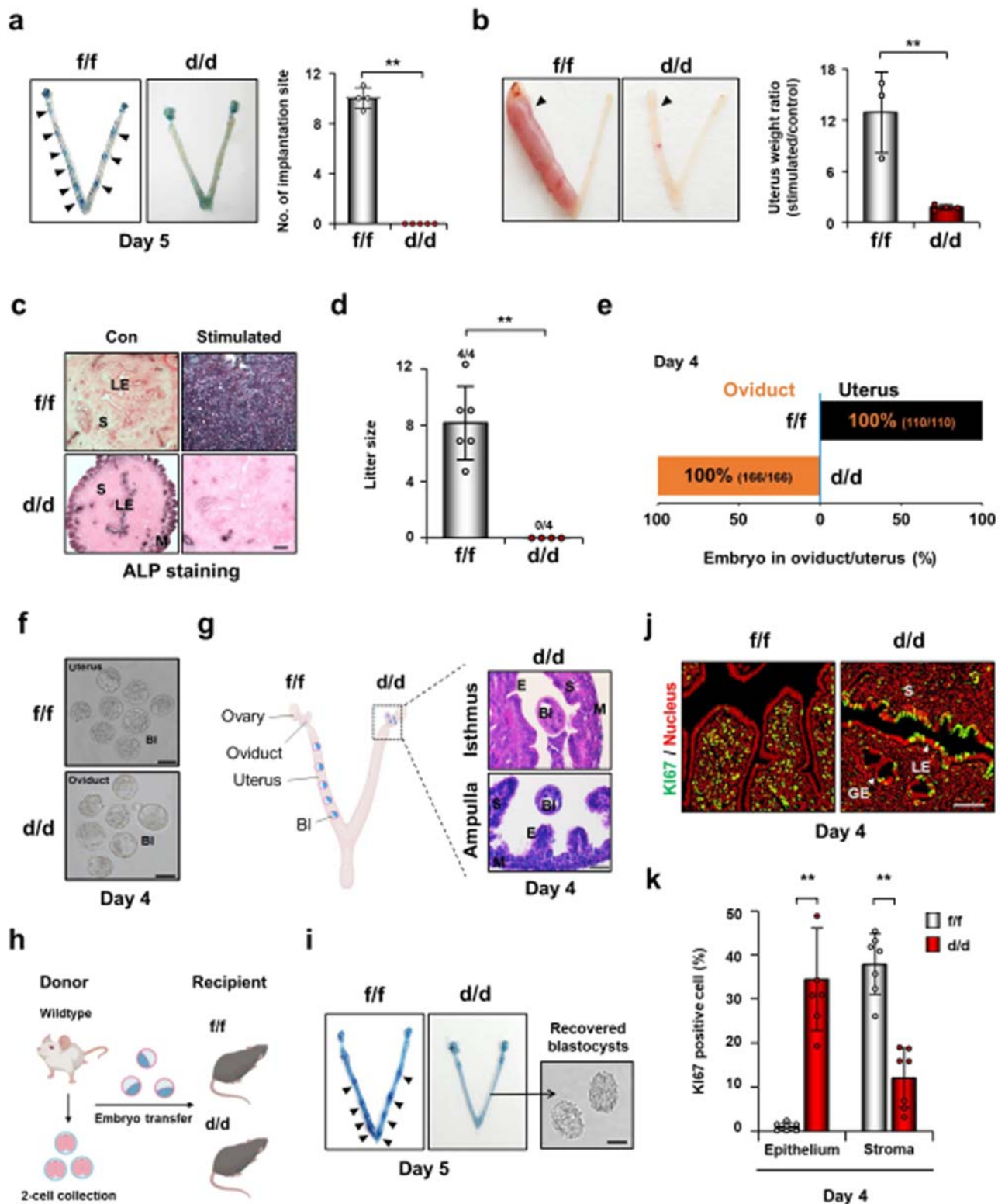
CFPI is expressed in many cells of female reproductive organs, such as the ovary, oviduct, and uterus (Supplementary Fig. 1). During early

pregnancy, uterine CFPI expression gradually increased from day 1 of pregnancy (Day 1) to Day 3. It peaked on Day 4, with the highest expression in the luminal epithelium. However, its expression is not directly affected by the regulation of E₂ and/or P₄ in the mouse uterus (Supplementary Fig. 1). While *Cfp1* is deleted in most cell types in the female reproductive tract of adult *Cfp1^{fl/fl};Pgr^{cre/+}* (*Cfp1^{d/d}*) mice (Supplementary Fig. 2), they showed normal architectures in the gross morphology and histology of the reproductive tract with regular estrous cycle (Supplementary Fig. 3a–c). Furthermore, serum levels of E₂ and P₄ on Day 4 in *Cfp1^{d/d}* mice were comparable to those of *Cfp1^{fl/fl}* mice. We also found that *Cfp1^{d/d}* mice ovulate similar numbers of oocytes that can fertilize normally, and the fertilized embryos develop to the blastocyst stage without any aberrations in vitro (Supplementary Fig. 3d–f). However, implantation sites (IS), blue bands along the uterus, were not observed in *Cfp1^{d/d}* female mice on Day 5 (Fig. 1a). In addition, *Cfp1^{d/d}* uteri did not show decidual responses to artificial stimuli, such as oil (Fig. 1b, c). Accordingly, *Cfp1^{d/d}* female mice did not produce any pups (Fig. 1d). Interestingly, all blastocysts were found in the oviduct but not in the uterus of *Cfp1^{d/d}* mice on Day 4, whereas they were found in the uterus of *Cfp1^{fl/fl}* mice as expected (Fig. 1e–g).

To examine embryo implantation in the uterus of *Cfp1^{d/d}* mice with defective oviductal embryo transport, wildtype blastocysts were transferred to the uteri of *Cfp1^{fl/fl}* and *Cfp1^{d/d}* mice on day 4 of pseudopregnancy. Distinct IS were observed in *Cfp1^{fl/fl}* but not in *Cfp1^{d/d}* recipients, and unimplanted blastocysts were retrieved from *Cfp1^{d/d}* recipients 24 h after embryo transfer (Fig. 1h, i and Table 1), indicating that CFPI-deficient uterine environments do not support embryo implantation. In this aspect, cell proliferation profiles are aberrant in the uterus of *Cfp1^{d/d}* mice on Day 4 (Fig. 1j, k), whereas the levels of E₂ and P₄ (Supplementary Fig. 3d) and their receptors (Supplementary Fig. 4) are comparable between *Cfp1^{fl/fl}* and *Cfp1^{d/d}* mice. Nevertheless, the uterine epithelium persistently proliferates, and the stroma showed less proliferation potential in the uterus of *Cfp1^{d/d}* mice, suggesting that CFPI, as an epigenetic regulator, is required for proper hormone responses in the uterus for a successful pregnancy.

CFPI regulates uterine mRNA landscapes in both H3K4me₃-dependent and H3K4me₃-independent manners

To understand the CFPI-dependent epigenetic regulation on transcriptional landscapes in the uterus, we performed chromatin immunoprecipitation sequencing (ChIP-seq) and mRNA sequencing (mRNA-seq) with the uteri of *Cfp1^{fl/fl}* and/or *Cfp1^{d/d}* mice on Day 4 (Fig. 2). ChIP-seq with antibodies for CFPI and H3K4me₃ provided evidence that CFPI-binding sites are highly enriched in TSS and CGI, and H3K4me₃ in TSS and CGI was generally reduced in the uterus of *Cfp1^{d/d}* mouse (Fig. 2a). De novo motif analysis for CFPI ChIP-seq data showed that CFPI recognizes the CCGG motifs, including CGG and its reverse complement CCG (Fig. 2b), which are consistent with the CFPI-binding motifs found in humans^{30–32}. CFPI binding was noticeably enriched in extended gene bodies, including promoters (9%), exons (4%), and introns (38%) in mouse uterus, considering that the mouse genome consists of promoters (2%), exons (2%), introns (20%), and intergenic factors (76%) (Fig. 2c). When the mRNA-seq and H3K4me₃ ChIP-seq data in ±2 kilo base pairs (Kbp) of TSS were analyzed together, 40.3% of differentially expressed genes (DEGs) had a reduction in both gene expression and H3K4me₃ levels in *Cfp1^{d/d}* mice (Fig. 2d) as expected from the known actions of CFPI on H3K4me₃. Generally, the lower gene expression levels are, the lower the H3K4me₃ levels in the +2Kbp TSS region are (Supplementary Fig. 5). However, a significant portion of DEGs (18.2%) was made up of genes with decreased expression levels and increased H3K4me₃ levels in *Cfp1^{d/d}* mouse uterus on Day 4, suggesting that CFPI could promote gene expression in the uterus in H3K4me₃-independent manner.



Although CFP1 binds to unmethylated CpG and induces H3K4me3 to increase gene expression¹³, the number of significantly downregulated (3329) and upregulated (2829) genes in *Cfp1*^{d/d} mice was comparable (54% vs. 46%) in DEGs from mRNA-seq (Fig. 2e and Supplementary Fig. 6a). However, gene ontology (GO) analyses showed that most GO terms (126/132, 95.5%) with false discovery rate (FDR) of <0.25 were reduced in the uteri of *Cfp1*^{d/d} mice on Day 4 (Fig. 2f and Supplementary Fig. 6b). Gene set enrichment analyses (GSEA) showed that various gene sets associated with P₄ response, hedgehog

signaling, cancers, ion channel activities, and stromal cell stimulation were significantly downregulated in *Cfp1*^{d/d} uterus (Fig. 2g). Interestingly, the Indian hedgehog (IHH)-dependent smoothed signaling pathway (SSP) is a well-known P₄ downstream pathway that inhibits E₂-dependent epithelial proliferation and further stimulates stromal proliferation in the uterus³³. A heatmap, reverse-transcriptase polymerase chain reaction (RT-PCR), and real-time RT-PCR analyses for the SSP gene set validated that IHH-dependent SSP is significantly downregulated in *Cfp1*^{d/d} mouse uterus on Day 4 (Fig. 2h, i).

Fig. 1 | *Cfp1^{dl/dl}* mice suffer from aberrant epithelial cell proliferation and complete failure of embryo implantation and decidualization. **a** Representative photographs of uteri with IS (black arrowheads) in *Cfp1^{fl/fl}* and *Cfp1^{dl/dl}* mice on Day 5. $n = 4$ to 5 biologically independent samples per genotype. Data are presented as mean values with SD. Statistical analyses were performed using the unpaired Student's *t*-tests. $**p < 0.01$. **b** Artificial decidualization responses in hormone primed *Cfp1^{fl/fl}* and *Cfp1^{dl/dl}* OVX mice. The decidual response was determined by the uterine weight of the oil-injected (black arrowheads)/non-injected uterine horn. $n = 3$ to 4 biologically independent samples per genotype. Data are presented as mean values with SD. Statistical analyses were performed using the unpaired Student's *t*-tests. $**p < 0.01$. **c** Microscopic images of alkaline phosphatase staining of artificially decidualized *Cfp1^{fl/fl}* and *Cfp1^{dl/dl}* uteri. Scale bar, 100 μm . **d** Litter size of *Cfp1^{fl/fl}* and *Cfp1^{dl/dl}* female mice that were mated with fertile male mice for 8–10 weeks. The numbers above the bars indicate the number of mice with litter/total number of mice examined in each group. Data are presented as mean values with SD. Statistical analyses were performed using the unpaired Student's *t*-tests. $**p < 0.01$.

e–h Impairment of the embryo transport from the oviduct to the uterus in *Cfp1^{dl/dl}* female mice. Percentage graph (**e**) and microscopic images (**g**) of embryos recovered from uteri and/or oviducts in *Cfp1^{fl/fl}* and *Cfp1^{dl/dl}* mice on Day 4. Scale bar, 50 μm in (**f**). **g** Schematic image of *Cfp1^{dl/dl}* oviduct in the morning of Day 4. Representative histological images of *Cfp1^{dl/dl}* oviduct (ampulla and isthmus) where blastocysts were found even in the morning of Day 4. Scale bar, 50 μm . Figure was created with BioRender.com. **h** Experimental scheme of embryo transfer. **i** Representative photographs of uteri with IS (black arrowheads) in pseudopregnant *Cfp1^{fl/fl}* and *Cfp1^{dl/dl}* recipients after transferring wildtype blastocysts. Scale bars, 50 μm . Figure was created with BioRender.com. **j, k** Immunofluorescent staining of KI67 to examine uterine cell proliferation in *Cfp1^{fl/fl}* and *Cfp1^{dl/dl}* mice on Day 4. Scale bar, 50 μm . BI blastocyst, S stroma, M muscle cells, E epithelium, GE glandular epithelium, LE luminal epithelium. $n = 6$ to 7 biologically independent samples per genotype. Data are presented as mean values with SD. Statistical analyses were performed using the unpaired Student's *t*-tests. $**p < 0.01$.

Table 1 | Embryo implantation in pseudopregnant *Cfp1^{fl/fl}* and *Cfp1^{dl/dl}* recipients after blastocyst transfer

Genotype of embryo	Genotypes of recipients	No. of recipients (No. of transferred embryos)	No. of mice with IS (%)	No. of IS (%)	No. of blastocysts recovered (%)
Wildtype	<i>Cfp1^{fl/fl}</i>	5 (76)	5 (100.0)	7.2 \pm 1.9 (47.4)	N.A.
	<i>Cfp1^{dl/dl}</i>	8 (126)	0 (0.0)	0 (0.0)	0.4 \pm 0.7 (2.4)

No number, IS implantation site, N.A. not applicable.

CFP1 epigenetically regulates P₄ responses through the IHH-dependent SSP in mouse uterus

To further investigate the epigenetic actions of CFP1 in the uterus, we tried to identify CFP1 direct target genes by analyzing all sequencing data together. The CFP1 direct target gene candidates should have CFP1-binding site(s) and be downregulated in *Cfp1^{dl/dl}* uteri. We found that the putative direct target genes of CFP1 are regulated not only in H3K4me3-dependent (673 genes) but also inH3K4me3-independent (423 genes) manner (Fig. 3a and Supplementary Data 1–2). Interestingly, the upstream and downstream genes of IHH-dependent SSP were included in the list; *Ihh*, *Gli3*, and *Gata2* as H3K4me3-dependent and *Ptch1*, *Sox17*, and *Nr2f2* as H3K4me3-independent target genes (Fig. 3b and Supplementary Data 2). The expression of these genes was reduced with statistical significance in *Cfp1^{dl/dl}* mice (Figs. 2i and 3c). The visualization of sequencing data for *Gata2*, *Ihh*, and *Sox17* using Integrative Genomics Viewer demonstrated that they all have CFP1 binding sites, and their expression levels were significantly reduced in *Cfp1^{dl/dl}* uteri. However, H3K4me3 levels were decreased in extended gene bodies of *Gata2* and *Ihh*, but not in *Sox17* (Fig. 3d). Real-time ChIP PCR reinforced that SETD1 and H3K4me3 were enriched in the promoter regions of *Gata2* and *Ihh* but not in *Sox17*, whereas CFP1 is enriched in all of them in *Cfp1^{fl/fl}* uterus (Fig. 3e and Supplementary Table 1). In summary, CFP1 works with SETD1 to increase H3K4me3 in *Gata2* and *Ihh* promoters but not for *Sox17* promoter for their expression in the uterus.

P₄-PGR induces stromal cell proliferation and inhibits epithelial cell proliferation via the activation of SSP downstream of *Gata2*, *Sox17*, and *Ihh* in mouse uterus on Day 4 (Fig. 3b). However, P₄ could not inhibit E₂-dependent epithelial proliferation and facilitate stromal cell proliferation in the uteri of ovariectomized (OVX) *Cfp1^{dl/dl}* mice (Fig. 3f, g) in line with the results on Day 4 (Fig. 1k). Since defective SSP could cause aberrant cell proliferation in *Cfp1^{dl/dl}* uteri, we tried to rescue this phenotype with SAG, a smoothed agonist, in these mice. An intrauterine delivery of SAG successfully rescued aberrant epithelial proliferation in the uteri of OVX *Cfp1^{dl/dl}* mice treated with E₂ and P₄ (Fig. 3f and 3g). Furthermore, SAG significantly restored the decreased expression levels of genes in SSP and its downstream genes, such as *Gli1*, *Gli2*, *Nr2f2*, and *Hand2*, in *Cfp1^{dl/dl}* uteri to the levels in *Cfp1^{fl/fl}* uteri (Fig. 3h). When our mRNA-seq datasets were compared with other P₄-related transcriptomic data (GSE118264, GSE40661, and GSE178541)^{13,34,35},

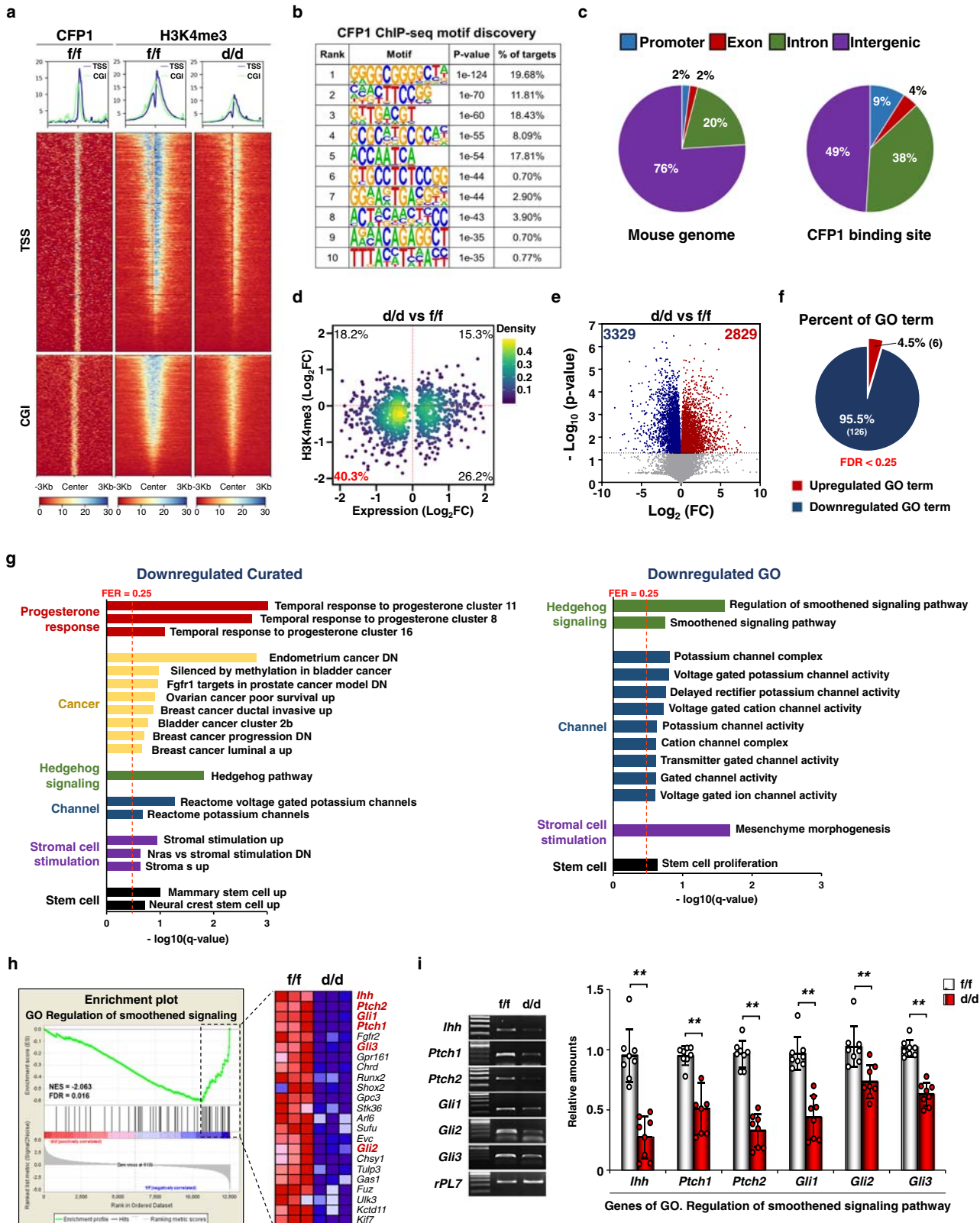
comparative analyses showed that significant numbers of DEGs in *Cfp1^{dl/dl}* uterus overlap with DEGs in other P₄-related datasets (Supplementary Fig. 7). Collectively, these results suggest that CFP1 loss disturbs the epigenetic maintenance of P₄-PGR signaling pathways in the uterus.

CFP1 is required for P₄ function to inhibit the growth of ectopic endometriotic lesions in mice

Endometriosis can occur possibly via a decreased P₄ response, and some patients with endometriosis show P₄ resistance even with normal *PGR* expression^{36–39}. To further evaluate CFP1 function for uterine P₄ responses, we established a mouse model of endometriosis with some modifications from previous reports^{25,26}. When P₄ was given with E₂, the size of ectopic lesions was significantly smaller than with E₂ alone, although the number of ectopic lesions was not different (Supplementary Fig. 8a, b). Ectopic lesions were mainly observed on organs with highly developed blood vessels, such as the small intestine, kidney, uterus, and fat pad (Supplementary Fig. 8c). When small pieces of *Cfp1^{fl/fl}* and *Cfp1^{dl/dl}* uterus as endometriotic lesions were transplanted to wildtype recipients (Fig. 4a), P₄ effectively suppressed the E₂-induced growth of *Cfp1^{fl/fl}* but not *Cfp1^{dl/dl}* ectopic lesions even if the number of ectopic lesions was not affected by *Cfp1* genotypes (Fig. 4b–e). The mRNA expression of *Gata2*, *Sox17*, and *Ihh* was also significantly downregulated in *Cfp1^{dl/dl}* ectopic uterine lesions (Fig. 4f). When SAG was administered to rescue P₄ resistance and/or insensitivity in *Cfp1^{dl/dl}* ectopic uterine lesions, P₄ suppressed the size of *Cfp1^{dl/dl}* ectopic lesions in the endometriosis model (Fig. 4b–e), suggesting that CFP1 is required for proper P₄ responses to suppress ectopic growth of uterine tissues in mice.

Downregulation of the epigenetic factor CFP1 may be associated with endometriosis in humans

To further evaluate the potential actions of CFP1 on the pathogenesis of endometriosis in humans, we analyzed datasets (GSE51981) of the endometria of patients with endometriosis (endometriosis group, $n = 77$) and healthy women (control group, $n = 71$) from a previous study⁴⁰. While no correlation exists between the expression levels of CFP1 and *PGR* mRNAs, *GATA2*, *SOX17*, and *IHH* mRNA expression levels were positively correlated with that of CFP1 (Fig. 5a) and *PGR* mRNA (Supplementary Fig. 9a) regardless of endometrial pathologic



conditions. We further analyzed a subset of GSE51981, i.e., endometria of women with mild and severe endometriosis in the mid-secretory phase where P₄ is dominant (Fig. 5b). In patients with mild endometriosis, the expression profiles of *PGR*, *CFPI*, and P₄ target genes are not different from those of the control group. However, there was a statistically significant reduction in their expression levels in patients with severe endometriosis (Supplementary Fig. 9b). Among patients with

severe endometriosis, some had a comparable level of *PGR* but a low level of *CFPI* (circled red, Fig. 5b). In these patients, the expression patterns of *GATA2*, *SOX17*, and *IHH* mRNAs were significantly decreased. It suggests that aberrantly reduced expression of *CFPI* may be associated with endometriosis via abnormal P₄ response in patients with normal *PGR* expression. We also performed immunohistochemistry and real-time RT-PCR for these genes in endometrial samples

Fig. 2 | CFPI epigenetically regulates uterine transcriptome via H3K4me3 on Day 4. **a** Tag density of CFPI binding and H3K4me3 peaks were calculated on ± 3 Kbp window centered on TTS and CGI regions of all RefSeq (mm10) genes in *Cfp1^{fl/fl}* and/or *Cfp1^{d/d}* mouse uteri on Day 4 for heatmap and graph data. **b** CFPI-binding sequence logo of the top 10 motifs identified using de novo motif discovery. **c** Distribution of the genetic features across the mouse genome and CFPI-binding peaks in *Cfp1^{fl/fl}* mouse uterus on Day 4. **d** Correlation between H3K4me3 promoter (TSS ± 2 Kbp) enrichment conditions and gene expression in the mouse uterus on Day 4 (*Cfp1^{d/d}* versus *Cfp1^{fl/fl}*). Each dot represents a differentially expressed gene with statistical significance ($p < 0.05$, normalized data average, $\log_2 > 3$). **e** Volcano plot to compare expression profiles from the *Cfp1^{fl/fl}* vs. *Cfp1^{d/d}* in the uterus on Day

4. **f** Pie chart summarizing upregulated or GO term in *Cfp1^{fl/fl}* versus *Cfp1^{d/d}* mouse uterus on Day 4. **g** GSEA to identify downregulated GO term and curated gene sets in *Cfp1^{fl/fl}* versus *Cfp1^{d/d}* mouse uterus on Day 4. Gene sets with an FDR q -value of < 0.25 (red dotted line) were considered significant. **h** GSEA enrichment plot and heatmap of the “GO Regulation of smoothed signaling” gene set from RNA-seq data of *Cfp1^{fl/fl}* and *Cfp1^{d/d}* mouse uterus on Day 4. The color spectrum from blue to red indicates low to high expression. **i** RT-PCR and Real-time RT-PCR analyses for *Ihh*-dependent SSP genes (red colored in **h**). $n = 8$ biologically independent samples per genotype. Data are presented as mean values with SD. Statistical analyses were performed using the unpaired Student's t -tests. $^{**}p < 0.01$.

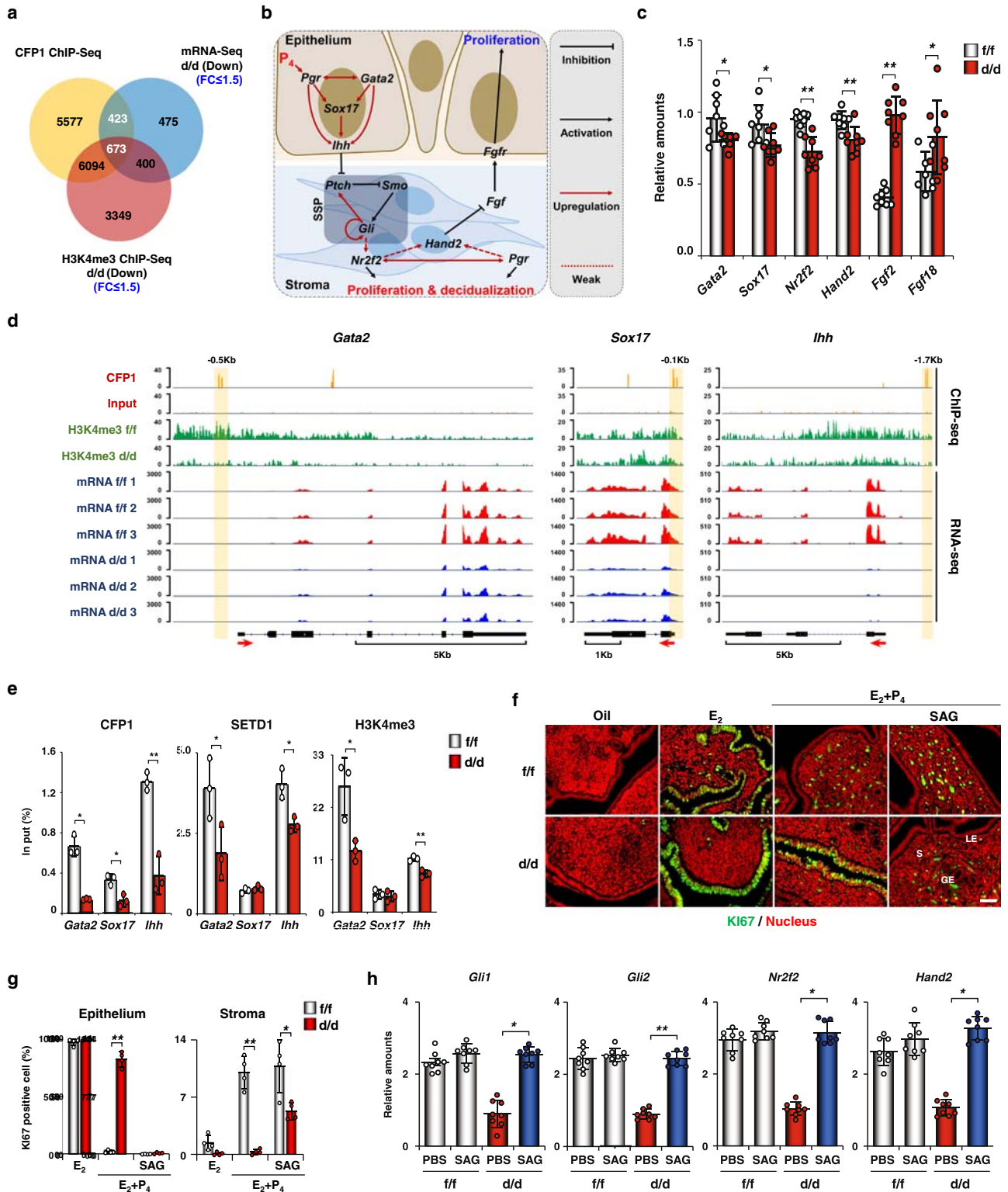
from patients with severe endometriosis and disease-free control women in the secretory phase. The eutopic and ectopic endometria from patients with endometriosis showed decreased expression levels of *CFPI*, *GATA2*, *SOX17*, and *IHH* mRNAs compared with the endometrium from the control group (Fig. 5c, d), suggesting that reduced CFPI expression may disturb epigenetic landscapes that mediate P₄-PGR signaling pathways in human endometrium, often leading to endometriosis.

Discussion

Many gynecological diseases are caused by abnormally reduced P₄ response; however, the underlying epigenetic aberration for the imbalanced steroid hormone responses has not been clearly elucidated. We demonstrate that CFPI-associated epigenetic regulation is required for maintaining appropriate P₄ responses for embryo implantation and decidualization in the uterus and inhibiting the ectopic growth of endometrial lesions outside the uterus. *Cfp1^{d/d}* mice exhibit a wide spectrum of infertility, including defective oviductal embryo transport, abnormal uterine cell proliferation, and complete failure of embryo implantation and decidualization (Fig. 1). These phenotypes suggest that epigenetic regulation through H3K4me3 is involved in the sequential events of female reproduction. A recent study supported those spatiotemporal dynamics of H3K4me3 in the uterine genome are needed to be well controlled for early pregnancy. In mice without MENIN (*Men1^{d/d}* mice), a member of the H3K4 methyltransferase complex, defective decidualization compromised fertility, whereas embryo implantation normally occurs⁴¹. Impaired decidualization in *Men1^{d/d}* mice was caused by reduced *Bmp2* expression by abnormally increased FGF2 signaling⁴¹. In *Cfp1^{d/d}* uterus on Day 4, *Fgf2* expression aberrantly increased because of a decrease in *Ihh*-dependent SSP that antagonizes FGF2 signaling, although the *Bmp2* expression did not decrease (Fig. 3). While MLL1/2 complexes that contain MENIN catalyze H3K4 methylation in a gene- and cell-specific manner, SETD1–CFPI complexes are the leading H3K4 methyltransferases among the six histone methyltransferases, SETD1A/B, MLL1/2, and MLL3/4^{9,41}. This is consistent with the fact that *Cfp1^{d/d}* mice show a wider spectrum of infertile phenotypes than *Men1^{d/d}* mice, suggesting that CFPI-dependent epigenetic regulation may work on the wider area of the genome. For example, we found an impairment of the oviductal embryo transport in *Cfp1^{d/d}* mice, which was not observed in *Men1^{d/d}* mice. Embryo transport in the oviduct could be interrupted by abnormalities in cilia movement, fluid secretion, and smooth muscle contraction^{42,43}. Since *Cfp1* was mainly deleted in non-ciliated epithelial cells of the isthmus, but not in ciliated ones, which are positive for acetylated tubulin in the ampulla of *Cfp1^{d/d}* oviduct by *Pgr*-Cre (Supplementary Fig. 2e, f), embryo retainment in the oviduct could result from abnormalities in fluid secretion and smooth muscle contraction⁴⁴, but not from cilia movement. While the epigenetic changes for fluid secretion are largely unknown, histone marks to promote transcription, such as H3K4me3 and H3K27 acetylation (H3K27ac), are enriched at promoters of genes driving muscle contraction on the advance of labor onset in the myometrium⁴⁵.

CFPI-dependent epigenetic regulation has been investigated in various biological events. The conditional deletion of *Cfp1* in mouse hematopoietic cells resulted in severe defects during hematopoiesis with complete loss of lineage-committed progenitors and mature cells⁴⁶. CFPI is also required for thymocyte survival, the balanced differentiation between Th17 and Treg cells^{7,8}, and the phagocytic and bactericidal activity of macrophages⁴⁷. Since *Pgr* is expressed in various immune cells, including macrophages⁴⁸, dendritic cells⁴⁹, and T cells⁵⁰, *Cfp1* was supposed to be deleted in immune cells as well as uterine cells in *Cfp1^{d/d}* mice. Immune cells play important roles during pregnancy⁵¹. However, immune-related gene sets were not significantly altered in *Cfp1^{d/d}* mouse uterus on Day 4 (Fig. 2g). Furthermore, normal fertility was observed in mice (*Cfp1^{fl/fl};LysM^{cre/+}*) in which *Cfp1* is deleted in the myeloid lineage cells, such as monocytes and macrophages, using *LysM*-Cre (Supplementary Table 2), suggesting that phenotypes observed in *Cfp1^{d/d}* mice are not directly associated with CFPI functions in immune cells. Recently, the function of CFPI–SETD1 complexes for epigenetic reprogramming during germ cell development has been investigated. CFPI-mediated H3K4me3 is required for maintaining chromatin accessibility for transcriptional activities during oocyte development, and oocyte-specific deletion of *Cfp1* caused reduced H3K4 methylation levels and globally downregulated transcription activities, in turn, leading to multiple defects in the meiotic division and maternal-to-zygotic transition¹⁰. Furthermore, CFPI participates in regulating the expression of paracrine factors for communication between the oocyte and surrounding granulosa cells for follicle growth and ovulation⁵². The conditional deletion of *Setd1b* in the oocyte also caused the dysregulation of transcription factors for oogenesis, including *Obox* transcription factors, leading to oocyte maturation defects and infertility⁵³. CFPI deletion before the onset of meiosis with *Stra8*-Cre in male mice caused complete infertility with the spermatogenic arrest at the MII stage¹¹, suggesting that CFPI-mediated H3K4me3 plays a role in meiosis and cell fate decision.

P₄ antagonizes E₂ action on epithelial proliferation and promotes stromal cell proliferation to prepare uterine receptivity for embryo implantation and decidualization^{13,54}. P₄ increased the expression of *Gata2*, *Sox17*, and *Ihh* in epithelial cells to trigger SSP in the stroma on Day 4 in mice^{13,33,34}, all of which were downregulated in *Cfp1^{d/d}* mice (Figs. 2 and 3). As a result, uterine epithelial cells aberrantly proliferated and failed to prepare embryo implantation on Day 4 in *Cfp1^{d/d}* mice (Fig. 1). The expression of gene sets related to P₄ response, *Ihh*-dependent SSP, and stromal cell stimulation was significantly reduced in *Cfp1^{d/d}* mice (Fig. 2g). Furthermore, SAG successfully rescued abnormal uterine cell proliferation in *Cfp1^{d/d}* mouse uterus (Fig. 3). They all indicate that disturbed P₄-PGR–SSP signaling pathway is the main cause of complete failure of embryo implantation and decidualization in *Cfp1^{d/d}* mice. In fact, mice without *Gata2*, *Sox17*, or *Ihh* phenocopied all these uterine defects observed in *Cfp1^{d/d}* mice^{13,33,34}. In addition, SAG restored decidualization and abnormal uterine cell proliferation in *Ihh* cKO mice³³. PGR is decreased in *Gata2*-deficient uteri, but it is necessary to mention that mice deficient in *Sox17*, *Ihh*, or *Cfp1* had normal PGR expression. Although reduced PGR expression



appears to be the main cause of P₄ resistance that contributes to the pathogenesis of endometriosis^{29,38,55}, some studies have reported comparable levels of PGR in eutopic^{36,38} or ectopic⁵⁶ endometria of women with endometriosis. This suggests that the epigenetic aberration in PGR downstream pathways could be involved in the pathogenesis of endometriosis⁵⁷. Essentially, the activation of PGR downstream pathways with SAG rescued the abnormal epithelial proliferation in *Cfp1*^{d/d} uterus (Fig. 3) and suppressed the ectopic growth of *Cfp1*^{d/d} uterine lesions with P₄ resistance in the endometriosis model

(Fig. 4). Aberrant epithelial proliferation was also found in the endometrium of patients with endometriosis^{25,58}. Considering impaired P₄-PGR signaling without PGR reduction (Supplementary Fig. 4) in *Cfp1*^{d/d} mice reflects P₄ resistance, disturbed CFP1-associated H3K4me3 could contribute to P₄ resistance that often leads to endometriosis in humans.

CFP1 mainly works to increase the expression of target genes through H3K4me3-dependent manners^{7,52}. Accordingly, 40.3% of DEGs in *Cfp1*^{d/d} uteri were downregulated with reduced H3K4me3

Fig. 3 | CFPI-dependent epigenetic regulation intervenes in important uterine P₄ responses via H3K4me3-dependent and H3K4me3-independent manners in mice. **a** Venn diagram of identifying genes that overlapped in datasets between CFPI-binding sites on their extended gene bodies (2 Kbp upstream and 200 bp downstream of TSS and CGI), downregulated gene in *Cfp1^{td/d}* mice (>1.5 folds), and downregulated H3K4me3 sites in *Cfp1^{td/d}* mice (>1.5 folds) on Day 4. **b** Schematic cartoon to show the epithelium–stroma crosstalk mediated by SSP. **c** Real-time RT-PCR analyses of upstream and downstream genes in IHH-dependent SSP (*Gata2*, *Sox17*, *Nr2f2*, *Hand2*, *Fgf2*, and *Fgf18*). *n* = 8 biologically independent samples per genotype. Data are presented as mean values with SD. Statistical analyses were performed using the unpaired Student's *t*-tests. **p* < 0.05, ***p* < 0.01. **d** Integrative Genomics Viewer screenshots that show the distribution of CFPI binding, H3K4me3 site, and RNA expression intensity in *Gata2*, *Sox17*, and *Ihh* of *Cfp1^{fl/fl}* and *Cfp1^{td/d}* mouse uterus on Day 4. **e** Real-time ChIP PCR for detecting CFPI, SETD1, and H3K4me3, binding on *Gata2*, *Sox17*, and *Ihh* in the uterus of *Cfp1^{fl/fl}* and *Cfp1^{td/d}* mice

on Day 4. *n* = 3 biologically independent samples per genotype. Data are presented as mean values with SD. Statistical analyses were performed using the unpaired Student's *t*-tests. **p* < 0.05, ***p* < 0.01. **f** Immunofluorescent staining of KI67 in the uterus of the OVX *Cfp1^{fl/fl}* and *Cfp1^{td/d}* mice treated with E₂ and/or P₄ for 24 h. At 3 h after E₂ or E₂ + P₄, one uterine horn was injected with SAG and the other one with PBS. Green and red indicate KI-67 and the nucleus, respectively. S stroma, GE glandular epithelium, LE luminal epithelium. Scale bar, 50 μm. **g** Percentages of KI67-positive cells in (f). *n* = 4 biologically independent samples per genotype. Data are presented as mean values with SD. Statistical analyses were performed using the unpaired Student's *t*-tests. **p* < 0.05, ***p* < 0.01. **h** Real-time RT-PCR analyses of SSP genes (*Gli1*, *Gli2*, *Nr2f2*, and *Hand2*) 3 h after SAG injection. *n* = 8 biologically independent samples per genotype. Data are presented as mean values with SD. Statistical analyses were performed using the multiple comparisons. **p* < 0.05, ***p* < 0.01.

levels (Fig. 2d). However, a substantial portion of downregulated DEGs had even higher H3K4me3 levels (18.2%). Although CFPI is an evolutionally conserved epigenetic regulator to work with SETDs for H3K4me3 from yeast to mammals, recent studies have suggested that CFPI could collaborate with epigenetic modulators other than COMPASS (complex associated with SET1) complexes, such as DNA methyltransferases (DNMTs) and HDACs, in a context-dependent manner. When CFPI/SETD1 or MLL1/2 binds to DNA, they hamper DNA methylation by blocking the access of DNMT3A⁵⁹. CFPI interacts with and recruits DNMT1 to suppress aberrant transcription re-initiation or silence specific genes^{2,60}. The expression of *Dnmt1* and *Dnmt3a* increased gradually in the mouse uterus during early pregnancy⁶¹. They suggest that the H3K4me3-independent gene expression in *Cfp1^{td/d}* uteri could be associated with reduced DNA methylation. In addition to DNMTs, CFPI could interact with HDAC1/2 complexes to regulate fertility and development in *C. elegans*. CFPI recruits the HDAC complex to H3K4me3-rich promoter regions to deacetylate chromatin⁶². CFPI-dependent H3K4me3 is necessary to recruit histone acetylase(s) for H3K9ac dynamics in mouse embryonic stem cells⁶, suggesting that CFPI-associated H3K4me3 cross-talks with histone acetylation. Interestingly, higher P₄ levels in in vitro fertilization cycles on the day of hCG administration altered various epigenetic marks, including H3K9ac, H3K9me2, and H3K27me3, in the endometrium⁶³, suggesting that histone modifications and P₄-PGR signaling influence each other in the endometrium. The epithelial cells in endometriotic lesions expressed a higher level of EZH2, the enzyme responsible for a repressive mark H3K27me3, which P₄ upregulates⁶⁴. MLL1 is directly regulated by P₄-PGR signaling in the uterus and MLL1 and H3K4me3 both decreased in the eutopic endometrium of patients with endometriosis⁶⁵. Furthermore, the expression of HDAC3, one of HDACs that reduce gene expression, was significantly lower in the endometrium of patients with endometriosis. The loss of HDAC3 in mice leads to infertility that results from embryo implantation failures with defective decidualization possibly through the aberrant activation of *Col1a1* and *Col1a2* genes that promote fibrosis with decreased ESR and PGR in the uterus²⁵. In summary, our results suggest that aberrant epigenetic regulation in CFPI-deficient mice provides a uterine environment with P₄ resistance that leads to infertility caused by multiple failures and endometriosis (Fig. 6). This study is of great significance to provide an underlying epigenetic mechanism of P₄ resistance in the endometrium that could lead to endometriosis in humans.

Methods

Animals

All mice used in this study were maintained in accordance with the policies of the CHA University Institutional Animal Care and Use Committee (No150083). Adult (8–10 weeks of age) C57BL/6 mice, provided by Orient Bio (Gapyeong, Gyeonggi, Korea), were housed

under temperature- and light-controlled conditions with the light on for 12 h daily and fed ad libitum. *Cfp1^{fl/fl}* mice were kindly provided by Dr. David G. Shkolnik's laboratory¹. First, *Cfp1^{fl/fl}* mice were mated to *Pgr^{cre/+}* mice to generate *Cfp1^{fl/+};Pgr^{cre/+}* mice⁶⁶. Then, these mice were crossed to generate *Cfp1^{td/d}* and *Cfp1^{fl/fl}* mice. Genotyping PCR was performed by genomic DNA extracts from tail biopsies (Supplementary Table 3).

Vaginal smear analysis and fertility test

Estrous cyclicity was evaluated in mature *Cfp1^{fl/fl}* and *Cfp1^{td/d}* female mice by daily analysis of vaginal smears over 2 weeks between 8:00 and 9:00 AM. The estrous cycle stage (proestrus, estrus, metestrus, and diestrus) was determined based on the presence of vaginal cornified epithelial cells and nucleated epithelial cells/total vaginal cells. To evaluate reproductive performance, mature *Cfp1^{fl/fl}* and *Cfp1^{td/d}* female mice (*n* = 4 per genotype) were individually bred to wildtype males with proven fertility. The numbers of litters and pups were recorded for 2 months.

Serum E₂ and P₄ level measurement

Blood samples were collected on Day 4 (9:00 AM) from the heart of *Cfp1^{fl/fl}* and *Cfp1^{td/d}* female mice (*n* = 5 to 9 per genotype). First, the mouse blood was sampled without anticoagulant and transferred to a sterile empty tube. Next, the mouse blood was centrifuged at 1500 × *g* for 15 min at 4 °C. Separated serum was transferred into a new sterile empty tube. Serum levels of mouse E₂ and P₄ were measured by radioimmunoassay⁶⁷.

Ovulation, fertilization, and preimplantation embryo development

Cfp1^{fl/fl} and *Cfp1^{td/d}* female mice were bred to wildtype males with known fertility. The morning of the vaginal plug observation was designated as Day 1. The mice were sacrificed on Day 2, and their oviducts were flushed to evaluate the number and fertilization potential of ovulated oocytes (*n* = 7 per genotype). In addition, fertilized 2-cell embryos were cultured up to the blastocyst stage in 20 ml droplets of KSOM (Millipore, Danvers, MA, USA) covered with oil (SAGE In-Vitro Fertilization, Inc., Trumbull, CT, USA) in a petri dish.

Hormone treatments

To investigate time-dependent actions of E₂ or P₄ on the expression of *Cfp1* in C57BL/6 mice uterus, adult (8–10 weeks of age) female mice were OVX, rested for 14 days, and then subcutaneously injected with either vehicle (sesame oil, 0.1 mL/mouse; Acros, NJ, USA), E₂ (100 ng/mouse, Sigma-Aldrich, St. Louis, MO, USA) or E₂ + P₄ (2 mg/mouse, Sigma-Aldrich). After hormone injection, the mice were sacrificed at various time points (0–24 h) and the uterus was collected for real-time RT-PCR (*n* = 4 to 6 per each group).

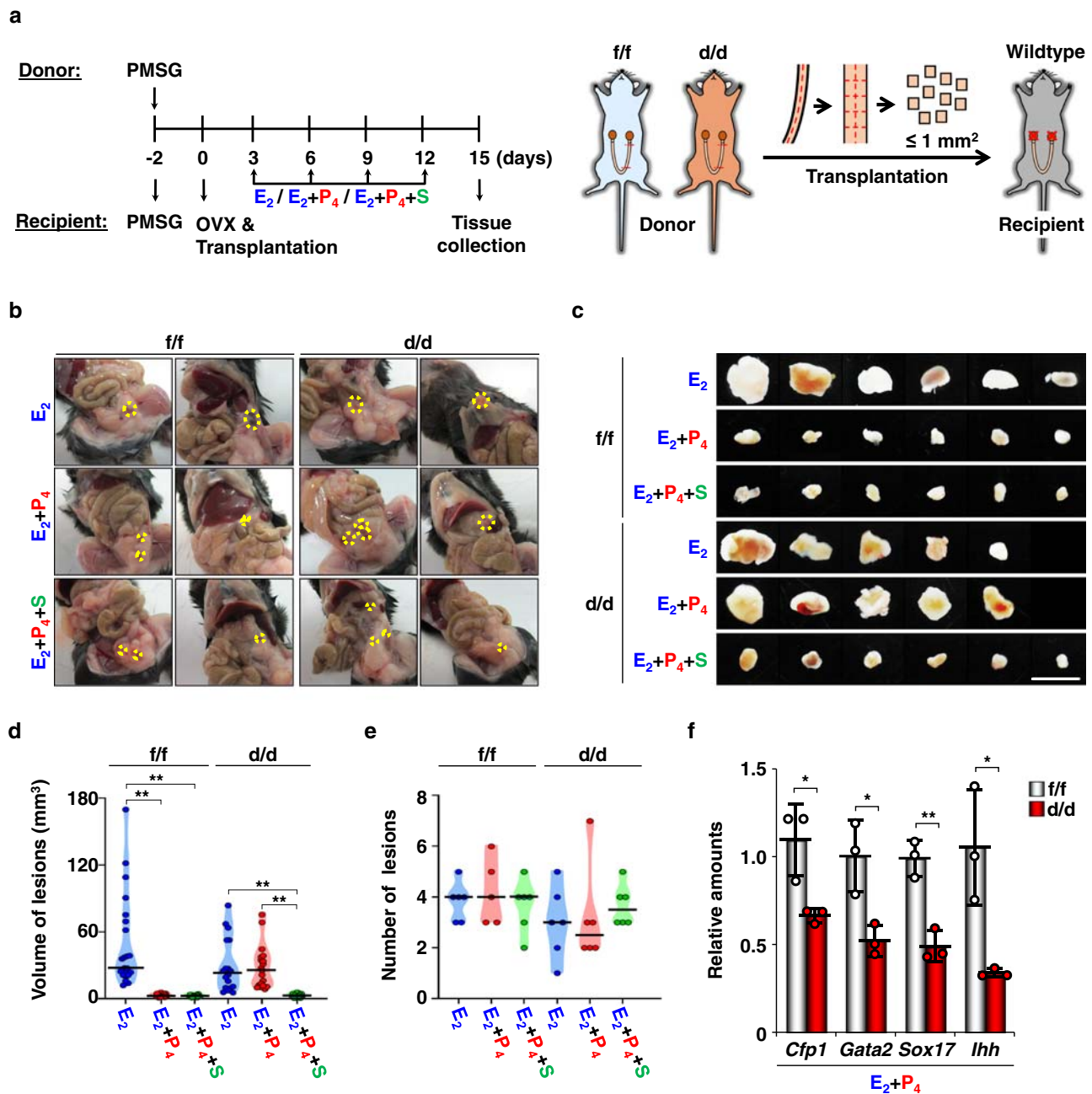


Fig. 4 | CFPI is required for the counteraction of P_4 on E_2 -dependent uterine growth in a mouse model of human endometriosis. a Schematic protocol to induce an experimental model of human endometriosis with transplantation of $Cfp1^{f/f}$ or $Cfp1^{d/d}$ uterine fragments. **b–e** Representative photographs to show the in vivo locations (**b**) and size (**c**) of ectopic lesions (dashed circles) harvested 15 days after transplantation of small pieces of $Cfp1^{f/f}$ and $Cfp1^{d/d}$ uterine tissues in recipients treated with E_2 , $E_2 + P_4 + PBS$, or $E_2 + P_4 + SAG$. Scale bar, 5 mm. Average

volumes (**d**) and numbers (**e**) of ectopic lesions collected from recipients. $n = 5$ to 6 biologically independent samples per group. Statistical analyses were performed using the multiple comparisons. $*p < 0.05$, $**p < 0.01$. **f** Real-time RT-PCR analyses of $Cfp1$, $Gata2$, $Sox17$, and Ihh expression in $Cfp1^{f/f}$ and $Cfp1^{d/d}$ ectopic uterine lesions in recipients treated with E_2 and P_4 . $n = 3$ biologically independent samples per genotype. Data are presented as mean values with SD. Statistical analyses were performed using the unpaired Student's t -tests. $*p < 0.05$, $**p < 0.01$.

Tissue preparation

Female reproductive organs under various conditions, such as early pregnancy, ovarian steroid hormone treatment, and artificial decidualization, were dissected and then fixed in 4% paraformaldehyde. Fixed tissues were washed, dehydrated, and embedded in paraplant (Merck KGaA, Darmstadt, Germany). Paraffin-embedded tissues were sectioned to 5 μm thickness using a microtome, stained with hematoxylin and eosin (Sigma–Aldrich), and observed by light microscopy.

Early pregnancy and embryo implantation

Pregnancy was evaluated by the presence of a vaginal plug on the next morning after breeding with a fertile male. The pregnant mice were sacrificed on various days of pregnancy from Day 1 to 5, and their uterine horns were collected and processed for the following experiments ($n = 4$ to 6 per each group). IS were detected by intravenous (i.v.) injection of 1% Chicago Sky Blue (in saline) on the morning of Day 5, and the number of IS demarcated by blue spots was recorded⁶⁸.

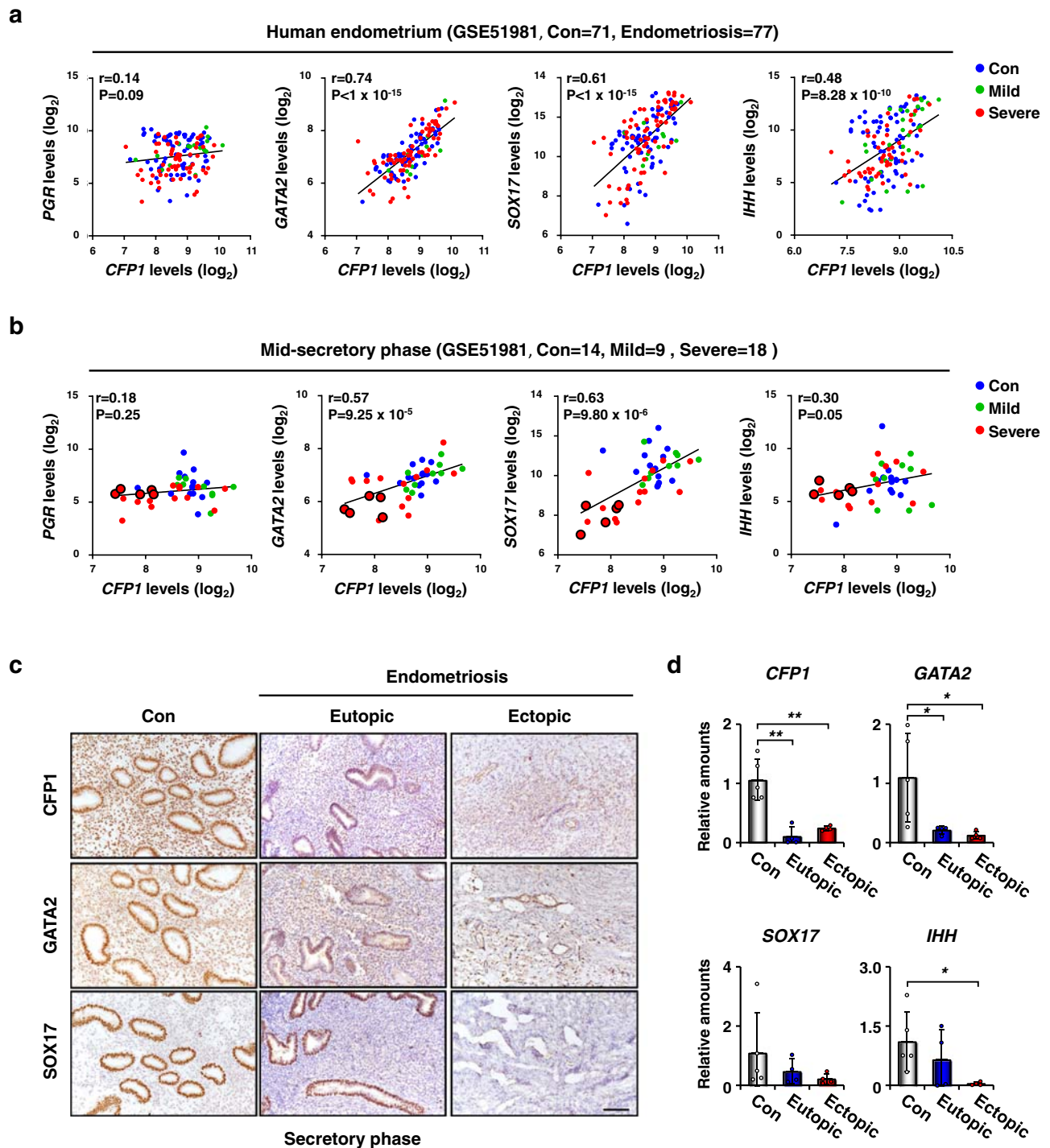


Fig. 5 | Concomitant reduction of *CFPI* and important P_4 responsive genes observed in the endometrium of patients with endometriosis. a Scatterplot of the positive correlations between mRNA expression levels of *CFPI* and important P_4 -responsive genes, *GATA2*, *SOX17*, and *IHH*, in human endometrium of healthy women (control, blue dots) and patients with mild (green) or severe (red) endometriosis (data from GSE51981). **b** Positive correlations were observed between the expression levels of *CFPI* and *GATA2*, *SOX17*, and *IHH* in the human endometrium in the med-secretory phase in (a). Note that a subgroup of patients with severe

endometriosis had lower expression of *CFPI* and important P_4 -responsive genes without *PGR* reduction (circled red dots). *r* indicates Pearson correlation coefficient. **c–d** Immunohistochemical staining (c) and real-time RT-PCR (d) of *CFPI*, *GATA2*, *SOX17*, and/or *IHH* in the human endometrium of healthy women (control) and patients with severe endometriosis (eutopic and ectopic) on the secretory phase. *n* = 4 to 5 biologically independent samples per group. Scale bar, 100 μ m. Data are presented as mean values with SD. Statistical analyses were performed using the multiple comparisons. **p* < 0.05, ***p* < 0.01.

Embryo transfer

Embryo transfer was performed as previously described with some modifications⁶⁹. Four-week-old C57BL/6 mice were given intraperitoneal (i.p.) injections of 5 IU PMSG (Sigma–Aldrich) followed by i.p.

injections with 5 IU hCG (Sigma–Aldrich) and then mated with fertile male mice to obtain the embryos for embryo transfers. The blastocysts were transferred to the uteri of either pseudopregnant day 4 *Cfp1*^{fl/fl} and *Cfp1*^{d/d} recipient mice, which were mated with vasectomized C57BL/6

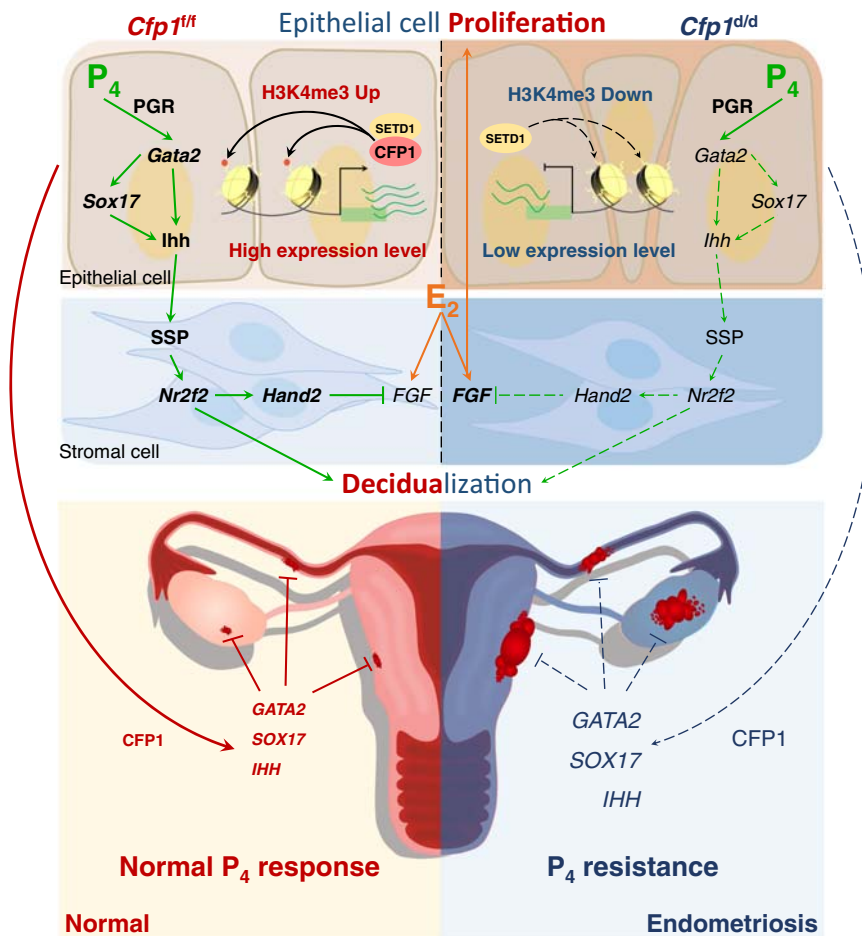


Fig. 6 | A schematic illustration of CFP1 function in P₄-epigenome-transcriptome networks for uterine physiology. CFP1 function to maintain P₄-PGR signaling for embryo implantation during early pregnancy and suppression of endometriosis in the uterus.

male mice. Embryo implantation was evaluated by an i.v. injection (0.1 mL/mouse) of Chicago Sky Blue (1% in saline, Sigma–Aldrich) 24 h after embryo transfer.

Artificial decidualization

Artificial decidualization was experimentally induced, as previously described, with some modifications⁶⁹. Adult (8–10 weeks of age) *Cfp1^{fl/fl}* and *Cfp1^{d/d}* female mice were OVX and rested for 14 days and then received daily injections of 100 ng E₂ for 3 days ($n = 3$ to 4 per genotype). After 2 days of resting, the mice were then treated with daily injections of 1 mg P₄ and 10 ng E₂ for 3 days. At 6 h after the last injection, one uterine horn was traumatized by the injection of 50 μ L of sesame oil. Mice were given daily injections of P₄ (1 mg) + E₂ (10 ng) following trauma. The weight of stimulated and non-stimulated uterine horns was recorded 4 days after the oil infusion. The fold increase in uterine weights and alkaline phosphatase staining served as an index of decidualization.

Intrauterine delivery of SAG

SAG (Abcam, Cambridge, UK), a smoothed agonist, was applied to rescue aberrant uterine cell proliferation and gene expression in *Cfp1^{d/d}* female mice³³. Adult (8–10 weeks of age) *Cfp1^{fl/fl}* and *Cfp1^{d/d}* female mice were OVX and rested for 14 days. Each OVX mouse was treated with 2 mg P₄ for 2 days and then 2 mg P₄ and E₂ 60 ng/mouse on the third day. At 3 h after E₂ and P₄ injection, 10 μ L of vehicle (PBS) and SAG (1000 nM) in PBS were injected intraluminally in each horn of the uterus. Mice were sacrificed at 3 or 21 h after SAG injection depending on experimental conditions, and the uterus was collected

for real-time RT-PCR and immunofluorescence staining ($n = 8$ per each group).

RNA extraction, RT-PCR, and real-time RT-PCR

Total RNA was extracted from mouse uteri under various conditions ($n = 3$ to 8 per each group) using Trizol Reagent (Invitrogen Life Technologies, San Diego, CA, USA) according to the manufacturer's protocols. The first-strand cDNA was synthesized from 1 μ g of total RNA using M-MLV reverse transcriptase (Promega, Madison, WI, USA) and RNasin Ribonuclease inhibitor (Promega). Synthesized cDNA (10 ng) was utilized for PCR with specific primers at optimized cycles (Supplementary Table 4). To quantify expression levels, real-time RT-PCR was performed using the SYBR green dye (iQ SYBR Green Supermix, Bio-Rad, Hercules, CA, USA), as previously described⁶⁸. To compare transcript levels between samples, a standard curve of cycle thresholds for several serial dilutions of a cDNA sample was established and then used to calculate the relative abundance of each gene. Then, values were normalized to the relative amounts of *Rpl7* cDNA. All reactions were performed in duplicates.

Western blotting

Uterus tissues ($n = 4$ to 6 per each group) were lysed in lysis buffer including PRO-PREP (iNtRON, Seongnam, Korea) solution and 1X phosphatase inhibitor (Roche Applied Sciences, Indianapolis, IN, USA). The protein samples (20 μ g/lane) were then separated by 8% SDS-PAGE, transferred onto nitrocellulose membrane (Bio-Rad), and blocked with 5% non-fat milk (Bio-Rad) in TBS (Bio-Rad) containing 0.1% Tween 20 (Sigma–Aldrich). Antibodies used for Western blotting,

immunostaining, and/or ChIP were summarized in Supplementary Tables 5 and 6. The signals were developed using an ECL Western blotting substrate kit (Bio-Rad) and detected using a Chemidoc XRS+ (Bio-Rad) with Image Lab software.

Immunohistochemistry and immunofluorescence analysis

Paraffin-embedded tissues were sectioned to 5 μm thickness using a microtome. Uterine sections were deparaffinized and rehydrated. Endogenous peroxidase was inactivated with 3% H_2O_2 . Sections were subjected to antigen retrieval in 0.01 M sodium citrate buffer (pH 6.0). Nonspecific staining was blocked using protein block serum (Dako, Carpinteria, CA, USA) for 1 h. Sections were incubated with primary antibodies at 4 °C overnight. On the following day, sections were incubated with appropriate secondary antibodies for 1 h at room temperature. Sections were counterstained using Topro-3-iodide (TOPRO; Life Technologies, Carlsbad, CA, USA) and mounted. For immunohistochemistry, DAB reagent (Vector Laboratories, Inc., Burlingame, CA, USA) was applied to visualize signals. Images were observed under a microscope (Carl Zeiss, Oberkochen, Germany) and analyzed using ZEN software (Carl Zeiss).

mRNA-seq and data analysis

Libraries were prepared from 2 μg of total RNA in *Cfp1^{fl/fl}* and *Cfp1^{dl/dl}* mouse uterus on Day 4 using the SMARTer stranded mRNA-Seq kit (Clontech Laboratories, Inc., USA). mRNAs were used for the cDNA synthesis and shearing, following the manufacturer's instructions ($n = 3$ pools: 3 mice per each pool). The Illumina indexes were used, and the enrichment step was conducted with PCR. The RT (read count) data were processed based on the quantile normalization method using EdgeR within R⁷⁰ utilizing bioconductor. The alignment files were also used for assembling transcripts, estimating their abundances, and detecting differential expression of genes or isoforms using cufflinks. These are performed using Bowtie2 software. We also used the fragments per kilobase of exon per million (FPKM) fragments to determine the expression levels of the gene regions. Gene classification was based on searches made by GSEA, and heatmaps of the unsupervised hierarchical clustering and DEGs were produced using MeV software.

CFP1 immunoprecipitation

Immunoprecipitation of CFP1 protein using CFP1 antibodies was performed with the manufacturer's instructions using immunoprecipitation kit (Abcam). In addition, CFP1 Western blotting following immunoprecipitation was performed to evaluate the specificity of CFP1 antibodies used for CFP1 ChIP-seq for *Cfp1^{fl/fl}* uterine samples (Supplementary Fig. 10). On Day 4, uterine horns of *Cfp1^{fl/fl}* and *Cfp1^{dl/dl}* mice were cut vertically, and epithelial and stromal cells were separated from the smooth muscles ($n = 4$ to 5 per each group). Then, tissues were incubated in a lysis buffer with protease inhibitors and mixed on a rocker at 4 °C for 1 h. The tissue extracts were transferred to a fresh tube, and a predetermined amount of antibodies was added on a rocker at 4 °C for 4 h. After antibody binding, protein A/G Sepharose beads were added on a rocker at 4 °C for 1 h. Next, protein A/G Sepharose beads were collected, washed, and eluted. The protein of interest was purified by low-speed centrifugation at 4 °C and used for Western blotting.

ChIP and real-time ChIP PCR

ChIP analysis was performed with a slight modification of the manufacturer's instructions using the ChIP-IT Express Enzymatic kit (Active Motif, Carlsbad, CA, USA). On Day 4, *Cfp1^{fl/fl}* and *Cfp1^{dl/dl}* mouse uterus horns were cut, and epithelial and stromal cells were separated from the uterine smooth muscles ($n = 3$ pools: 3 mice per each pool). Then, epithelial and stromal cells were fixed in DMEM high-glucose media containing 1% formaldehyde and then made into single cell slurry

through an electric homogenizer. DNA fragments between 150 and 500 bp were obtained by enzymatic shearing cocktail after lysis cell and nuclei isolation through lysis buffer and Dounce homogenizer. Antibodies were added in sheared chromatin, and immunoprecipitation was performed overnight at 4 °C. Immunoprecipitated DNA was utilized for real-time ChIP PCR with specific primers (Supplementary Table 1). To quantify the enrichment level in ChIP-seq data, real-time ChIP PCR was performed with iQTM SYBR Green Supermix (Bio-Rad) on BIO-RAD iCycler using immunoprecipitated DNA. All PCR reactions (10% input, CFP1, SETD1, H3K4me3, and normal IgG) were duplicated ($n = 3$ to 4 per each group).

ChIP-seq and data analysis

The library was constructed using NEBNext[®] UltraTM DNA Library Prep Kit for Illumina (New England Biolabs, UK) according to the manufacturer's instructions. Briefly, the chopped DNA was ligated with adaptors. After purification, the PCR reaction was conducted with adaptor-ligated DNA and index primer for multiplexing sequencing. The library was purified using magnetic beads to remove all reaction components. The library size was assessed by Agilent 2100 bioanalyzer (Agilent Technologies, Amstelveen, Netherlands). High-throughput sequencing was performed as paired-end 100 sequencing using HiSeq 2500 (Illumina, Inc. USA). ChIP-seq metaplots and heatmaps were analyzed using DeepTools software.

Experimentally induced mouse model of endometriosis

Recipient (wild type) and donor (*Cfp1^{fl/fl}* and *Cfp1^{dl/dl}*) female mice (8–10 weeks of age) were primed with 5 IU PMSG (Sigma-Aldrich) for 48 h to stimulate uterine growth. After inhalation anesthesia, the uterine horn was collected from donor mice and vertically opened with scissors in a petri dish containing warmed Dulbecco's phosphate-buffered saline (37 °C). The uterine horn was cut into small pieces of approximately 1 mm² and injected into the peritoneum of the OVX recipient mice. After transplantation of uterine tissues in recipient mice, E₂ (100 ng/mouse), P₄ (2 mg/mouse), PBS, and/or SAG were injected every 3 days. At 15 days after transplantation, the volume and number of ectopic lesions were measured, and ectopic lesions were collected for real-time RT-PCR.

Human endometrial sampling

Control ($n = 7$) and endometriotic endometrial tissues ($n = 5$) were collected from patients who underwent hysteroscopy-laparoscopy surgery to evaluate endometrial abnormalities, including endometriosis in the Department of Obstetrics and Gynecology of the First Affiliated Hospital of Xiamen University. The sample collection and studies reported here were approved by the ethics committee of Hospital of Xiamen University (XMY-2021KYSB044), and all participants signed the informed consent. Endometriotic lesions were obtained from women (aged 25–35 years) suffering from ovarian endometriosis, confirmed by laparoscopy and histopathology. These patients had regular menstrual cycles and were recruited without hormone treatment for at least 3 months before surgery. All samples were collected during the luteal phase of the menstrual cycle.

Statistical analysis

GraphPad Prism version 8 software (GraphPad Software, La Jolla, CA, USA) was used for statistical analyses. All values are represented as mean \pm standard deviation. Statistical analyses were performed using the unpaired Student's *t*-tests, and $p < 0.05$ was considered statistically significant.

Reporting summary

Further information on research design is available in the Nature Portfolio Reporting Summary linked to this article.

Data availability

Raw data files are deposited in the NCBI Gene Expression Omnibus database under Super Series accession number [GSE219104](#). The Supplementary Fig. 7 data re-analyzed in this study are available in the [GSE118264](#) database¹³, [GSE40661](#) database³⁴, and [GSE178541](#) database³⁵. All other data supporting the findings of this study are available within the paper and its Supplementary Information. Source data are provided with this paper.

References

- Voo, K. S., Carlone, D. L., Jacobsen, B. M., Flodin, A. & Skalnik, D. G. Cloning of a mammalian transcriptional activator that binds unmethylated CpG motifs and shares a CXXC domain with DNA methyltransferase, human trithorax, and methyl-CpG binding domain protein 1. *Mol. Cell. Biol.* **20**, 2108–2121 (2000).
- Yang, Y., Yang, Y., Chan, K. & Couture, J. F. Analyzing the impact of CFP1 mutational landscape on epigenetic signaling. *FASEB J.* **35**, e21790 (2021).
- Thomson, J. P. et al. CpG islands influence chromatin structure via the CpG-binding protein Cfp1. *Nature* **464**, 1082–1086 (2010).
- Carlone, D. L. et al. Reduced genomic cytosine methylation and defective cellular differentiation in embryonic stem cells lacking CpG binding protein. *Mol. Cell. Biol.* **25**, 4881–4891 (2005).
- Bledau, A. S. et al. The H3K4 methyltransferase Setd1a is first required at the epiblast stage, whereas Setd1b becomes essential after gastrulation. *Development* **141**, 1022–1035 (2014).
- Clouaire, T., Webb, S. & Bird, A. Cfp1 is required for gene expression-dependent H3K4 trimethylation and H3K9 acetylation in embryonic stem cells. *Genome Biol.* **15**, 451 (2014).
- Lin, F. et al. Epigenetic initiation of the TH17 differentiation program is promoted by Cxxc finger protein 1. *Sci. Adv.* **5**, eaax1608 (2019).
- Cao, W. et al. CXXC finger protein 1 is critical for T-cell intrathymic development through regulating H3K4 trimethylation. *Nat. Commun.* **7**, 11687 (2016).
- Sha, Q. Q. et al. CFP1 coordinates histone H3 lysine-4 trimethylation and meiotic cell cycle progression in mouse oocytes. *Nat. Commun.* **9**, 3477 (2018).
- Yu, C. et al. CFP1 regulates histone H3K4 trimethylation and developmental potential in mouse oocytes. *Cell Rep.* **20**, 1161–1172 (2017).
- Jiang, Y. et al. CXXC finger protein 1-mediated histone H3 lysine-4 trimethylation is essential for proper meiotic crossover formation in mice. *Development* **147**, dev183764 (2020).
- Brown, S. B. & Hankinson, S. E. Endogenous estrogens and the risk of breast, endometrial, and ovarian cancers. *Steroids* **99**, 8–10 (2015).
- Wang, X. et al. SOX17 regulates uterine epithelial-stromal cross-talk acting via a distal enhancer upstream of *Ihh*. *Nat. Commun.* **9**, 4421 (2018).
- Kong, S. et al. Epigenetic control of embryo-uterine crosstalk at peri-implantation. *Cell Mol. Life Sci.* **76**, 4813–4828 (2019).
- Retis-Resendiz, A. M. et al. The role of epigenetic mechanisms in the regulation of gene expression in the cyclical endometrium. *Clin. Epigenet.* **13**, 116 (2021).
- Bunkar, N., Pathak, N., Lohiya, N. K. & Mishra, P. K. Epigenetics: a key paradigm in reproductive health. *Clin. Exp. Reprod. Med.* **43**, 59–81 (2016).
- Grimaldi, G. et al. Down-regulation of the histone methyltransferase EZH2 contributes to the epigenetic programming of decidualizing human endometrial stromal cells. *Mol. Endocrinol.* **25**, 1892–1903 (2011).
- Tamura, I. et al. Genome-wide analysis of histone modifications in human endometrial stromal cells. *Mol. Endocrinol.* **28**, 1656–1669 (2014).
- Nancy, P. et al. H3K27me3 dynamics dictate evolving uterine states in pregnancy and parturition. *J. Clin. Invest.* **128**, 233–247 (2018).
- Monteiro, J. B. et al. Endometriosis is characterized by a distinct pattern of histone 3 and histone 4 lysine modifications. *Reprod. Sci.* **21**, 305–318 (2014).
- Zondervan, K. T., Becker, C. M. & Missmer, S. A. Endometriosis. *N. Engl. J. Med.* **382**, 1244–1256 (2020).
- Vannuccini, S., Clemenza, S., Rossi, M. & Petraglia, F. Hormonal treatments for endometriosis: the endocrine background. *Rev. Endocr. Metab. Disord.* **23**, 333–355 (2022).
- Saunders, P. T. K. & Horne, A. W. Endometriosis: etiology, pathobiology, and therapeutic prospects. *Cell* **184**, 2807–2824 (2021).
- Lee, D., Kim, S. K., Lee, J. R. & Jee, B. C. Management of endometriosis-related infertility: Considerations and treatment options. *Clin. Exp. Reprod. Med.* **47**, 1–11 (2020).
- Kim, T. H. et al. Loss of HDAC3 results in nonreceptive endometrium and female infertility. *Sci. Transl. Med.* **11**, eaaf7533 (2019).
- Li, Y. et al. Progesterone alleviates endometriosis via inhibition of uterine cell proliferation, inflammation and angiogenesis in an immunocompetent mouse model. *PLoS ONE* **11**, e0165347 (2016).
- Dizerega, G. S., Barber, D. L. & Hodgen, G. D. Endometriosis: role of ovarian steroids in initiation, maintenance, and suppression. *Fertil. Steril.* **33**, 649–653 (1980).
- Kitawaki, J. et al. Endometriosis: the pathophysiology as an estrogen-dependent disease. *J. Steroid Biochem. Mol. Biol.* **83**, 149–155 (2002).
- Marquardt, R. M., Kim, T. H., Shin, J. H. & Jeong, J. W. Progesterone and estrogen signaling in the endometrium: what goes wrong in endometriosis? *Int. J. Mol. Sci.* **20**, 3822 (2019).
- Liu, K. & Min, J. Structural basis for the recognition of non-methylated DNA by the CXXC domain. *J. Mol. Biol.* **432**, 1674–1686 (2020).
- Xu, C. et al. DNA sequence recognition of human CXXC domains and their structural determinants. *Structure* **26**, 85–95.e83 (2018).
- Xu, C., Bian, C., Lam, R., Dong, A. & Min, J. The structural basis for selective binding of non-methylated CpG islands by the CFP1 CXXC domain. *Nat. Commun.* **2**, 227 (2011).
- Lee, K. et al. Indian hedgehog is a major mediator of progesterone signaling in the mouse uterus. *Nat. Genet.* **38**, 1204–1209 (2006).
- Rubel, C. A. et al. A Gata2-dependent transcription network regulates uterine progesterone responsiveness and endometrial function. *Cell Rep.* **17**, 1414–1425 (2016).
- Li, R. et al. The role of epithelial progesterone receptor isoforms in embryo implantation. *iScience* **24**, 103487 (2021).
- Prentice, A. et al. Ovarian steroid receptor expression in endometriosis and in two potential parent epithelia: endometrium and peritoneal mesothelium. *Hum. Reprod.* **7**, 1318–1325 (1992).
- McKinnon, B., Mueller, M. & Montgomery, G. Progesterone resistance in endometriosis: an acquired property? *Trends Endocrinol. Metab.* **29**, 535–548 (2018).
- Patel, B. G., Rudnicki, M., Yu, J., Shu, Y. & Taylor, R. N. Progesterone resistance in endometriosis: origins, consequences and interventions. *Acta Obstet. Gynecol. Scand.* **96**, 623–632 (2017).
- Szukiewicz, D. et al. Estrogen- and progesterone (P4)-mediated epigenetic modifications of endometrial stromal cells (EnSCs) and/or mesenchymal stem/stromal cells (MSCs) in the etiopathogenesis of endometriosis. *Stem Cell Rev. Rep.* **17**, 1174–1193 (2021).
- Tamareis, J. S. et al. Molecular classification of endometriosis and disease stage using high-dimensional genomic data. *Endocrinology* **155**, 4986–4999 (2014).
- Liu, M. et al. Menin directs regionalized decidual transformation through epigenetically setting PTX3 to balance FGF and BMP signaling. *Nat. Commun.* **13**, 1006 (2022).
- Shi, D. et al. Celsr1 is required for the generation of polarity at multiple levels of the mouse oviduct. *Development* **141**, 4558–4568 (2014).

43. Wang, H. et al. Aberrant cannabinoid signaling impairs oviductal transport of embryos. *Nat. Med.* **10**, 1074–1080 (2004).
44. Li, S. & Winuthayanon, W. Oviduct: roles in fertilization and early embryo development. *J. Endocrinol.* **232**, R1–R26 (2017).
45. Shchuka, V. M. et al. The pregnant myometrium is epigenetically activated at contractility-driving gene loci prior to the onset of labor in mice. *PLoS Biol.* **18**, e3000710 (2020).
46. Chun, K. T. et al. The epigenetic regulator CXXC finger protein 1 is essential for murine hematopoiesis. *PLoS ONE* **9**, e113745 (2014).
47. Hui, Z. et al. Cxxc finger protein 1 positively regulates GM-CSF-derived macrophage phagocytosis through Csf2r α -mediated signaling. *Front. Immunol.* **9**, 1885 (2018).
48. Khan, K. N. et al. Estrogen and progesterone receptor expression in macrophages and regulation of hepatocyte growth factor by ovarian steroids in women with endometriosis. *Hum. Reprod.* **20**, 2004–2013 (2005).
49. Butts, C. L. et al. Inhibitory effects of progesterone differ in dendritic cells from female and male rodents. *Gen. Med.* **5**, 434–447 (2008).
50. Hughes, G. C., Clark, E. A. & Wong, A. H. The intracellular progesterone receptor regulates CD4⁺ T cells and T cell-dependent antibody responses. *J. Leukoc. Biol.* **93**, 369–375 (2013).
51. Lee, J. Y., Lee, M. & Lee, S. K. Role of endometrial immune cells in implantation. *Clin. Exp. Reprod. Med.* **38**, 119–125 (2011).
52. Sha, Q. Q. et al. CFP1-dependent histone H3K4 trimethylation in murine oocytes facilitates ovarian follicle recruitment and ovulation in a cell-nonautonomous manner. *Cell Mol. Life Sci.* **77**, 2997–3012 (2020).
53. Brici, D. et al. Setd1b, encoding a histone 3 lysine 4 methyltransferase, is a maternal effect gene required for the oogenic gene expression program. *Development* **144**, 2606–2617 (2017).
54. Li, Q. et al. The antiproliferative action of progesterone in uterine epithelium is mediated by Hand2. *Science* **331**, 912–916 (2011).
55. Al-Sabbagh, M., Lam, E. W. & Brosens, J. J. Mechanisms of endometrial progesterone resistance. *Mol. Cell Endocrinol.* **358**, 208–215 (2012).
56. Zanatta, A. et al. The relationship among HOXA10, estrogen receptor alpha, progesterone receptor, and progesterone receptor B proteins in rectosigmoid endometriosis: a tissue microarray study. *Reprod. Sci.* **22**, 31–37 (2015).
57. Zubrzycka, A., Zubrzycki, M., Perdas, E. & Zubrzycka, M. Genetic, epigenetic, and steroidogenic modulation mechanisms in endometriosis. *J. Clin. Med.* **9**, 1309 (2020).
58. Lessey, B. A. & Kim, J. J. Endometrial receptivity in the eutopic endometrium of women with endometriosis: it is affected, and let me show you why. *Fertil. Steril.* **108**, 19–27 (2017).
59. Smith, Z. D. & Meissner, A. DNA methylation: roles in mammalian development. *Nat. Rev. Genet.* **14**, 204–220 (2013).
60. Butler, J. S., Lee, J. H. & Skalnik, D. G. CFP1 interacts with DNMT1 independently of association with the Setd1 Histone H3K4 methyltransferase complexes. *DNA Cell Biol.* **27**, 533–543 (2008).
61. Gao, F. et al. Epigenetic changes through DNA methylation contribute to uterine stromal cell decidualization. *Endocrinology* **153**, 6078–6090 (2012).
62. Pokhrel, B., Chen, Y. & Biro, J. J. CFP-1 interacts with HDAC1/2 complexes in *C. elegans* development. *FEBS J.* **286**, 2490–2504 (2019).
63. Xiong, Y. et al. Effects of high progesterone level on the day of human chorionic gonadotrophin administration in in vitro fertilization cycles on epigenetic modification of endometrium in the peri-implantation period. *Fertil. Steril.* **108**, 269–276.e261 (2017).
64. Colon-Caraballo, M., Monteiro, J. B. & Flores, I. H3K27me3 is an epigenetic mark of relevance in endometriosis. *Reprod. Sci.* **22**, 1134–1142 (2015).
65. Wen, X. et al. Decreased mixed lineage leukemia 1 is involved in endometriosis-related infertility. *J. Mol. Endocrinol.* **66**, 45–57 (2021).
66. Soyal, S. M. et al. Cre-mediated recombination in cell lineages that express the progesterone receptor. *Genesis* **41**, 58–66 (2005).
67. Zhang, S. et al. Uterine Rbpj is required for embryonic-uterine orientation and decidual remodeling via Notch pathway-independent and -dependent mechanisms. *Cell Res.* **24**, 925–942 (2014).
68. Park, M. et al. Perivascular stem cell-derived cyclophilin A improves uterine environment with Asherman’s Syndrome via HIF1 α -dependent angiogenesis. *Mol. Ther.* **28**, 1818–1832 (2020).
69. Kim, H. R. et al. Estrogen induces EGR1 to fine-tune its actions on uterine epithelium by controlling PR signaling for successful embryo implantation. *FASEB J.* **32**, 1184–1195 (2018).
70. Nguefack-Tsague, G., Zucchini, W. & Fotso, S. Frequentist model averaging and applications to bernoulli trials. *Open J. Stat.* **6**, 545 (2016).

Acknowledgements

This research was supported by Basic Science Research Program through the National Research Foundation of Korea (NRF) funded by the Ministry of Education (NRF-2019R1A6A1A03032888 to H.S.), by the NRF grant funded by the Korea government (the Ministry of Science and ICT) (NRF-2015R1A2A2A01006714 to H.S., NRF-2020R1C1C1008317 to H.R.K., NRF-2020R1A2C2005012 to H.S., and NRF-2020R1A6A3A01100338 to M.P.), by Bio & Medical Technology Development Program of the NRF and funded by the Korean government (MSIT) (NRF-2022M3A9E4016936 to S.-H.H.).

Author contributions

S.C.Y. and H.S. conceived and designed the experiments. S.C.Y., M.P., H.L., P.W., C.P., G.L., Q.C., S.H.P., and Y.S.K. performed experiments. S.C.Y., M.P., K.-H.H., Y.C., F.J.D., J.P.L., D.G.S., H.J.L., S.-H.H., H.-R.K. and H.S. analyzed the results. S.C.Y., M.P., and H.S. discussed the results and wrote the manuscript.

Competing interests

The authors declare no competing interests.

Additional information

Supplementary information The online version contains supplementary material available at <https://doi.org/10.1038/s41467-023-39008-0>.

Correspondence and requests for materials should be addressed to Haengseok Song.

Peer review information *Nature Communications* thanks the anonymous reviewers for their contribution to the peer review of this work. A peer review file is available.

Reprints and permissions information is available at <http://www.nature.com/reprints>

Publisher’s note Springer Nature remains neutral with regard to jurisdictional claims in published maps and institutional affiliations.

Open Access This article is licensed under a Creative Commons Attribution 4.0 International License, which permits use, sharing, adaptation, distribution and reproduction in any medium or format, as long as you give appropriate credit to the original author(s) and the source, provide a link to the Creative Commons license, and indicate if changes were made. The images or other third party material in this article are included in the article's Creative Commons license, unless indicated otherwise in a credit line to the material. If material is not included in the article's Creative Commons license and your intended use is not permitted by statutory regulation or exceeds the permitted use, you will need to obtain permission directly from the copyright holder. To view a copy of this license, visit <http://creativecommons.org/licenses/by/4.0/>.

© The Author(s) 2023

¹Department of Biomedical Science, CHA University, Seongnam, Gyeonggi 13488, Korea. ²Department of Stem Cell and Regenerative Biotechnology, Konkuk University, Seoul 05029, Korea. ³Fujian Provincial Key Laboratory of Reproductive Health Research, Department of Obstetrics and Gynecology, The First Affiliated Hospital of Xiamen, School of Medicine, Xiamen University, Xiamen, Fujian 361102, China. ⁴Department of Reproductive and Developmental Biology Laboratory, National Institute of Environmental Health Sciences, Research Triangle Park, NC 12233, USA. ⁵Department of Molecular and Cellular Biology and Center for Reproductive Medicine, Baylor College of Medicine, Houston, TX 77030, USA. ⁶Department of Biology, School of Science, Indiana University-Purdue University Indianapolis, Indianapolis, IN 46202, USA. ⁷Department of Veterinary Science, Konkuk University, Seoul 05029, Korea. ⁸Department of Internal Medicine, School of Medicine, Kangwon National University, Chuncheon, Gangwon-do 24431, Korea. ⁹KW-Bio Co., Ltd, Wonju 26493, Korea. ¹⁰These authors contributed equally: Seung Chel Yang, Mira Park. ✉e-mail: hssong@cha.ac.kr